8. Y. Saito, T. Yoshikawa, S. Banndow, M. Tomita, T. Hayashi, *Phys. Rev. B* **48**, 1907 (1993).
9. W. Ruland, in *Chemistry and Physics of Carbon*, P. L. Walker Jr., Ed. (Dekker, New York, 1968), p. 1.
10. B. E. Warren, *Phys. Rev.* **59**, 693 (1941); J. Biscoe and B. E. Warren, *Appl. Phys.* **13**, 364 (1942).
11. R. E. Franklin, *Acta. Crystallogr.* **3**, 107 (1950); *ibid.* **4**, 253 (1950).
12. The relation between radial and longitudinal compressibilities is derived here for a zigzag (n, 0) tube. In this geometry, the radius of the ith shell of the tube, r_i, is equal to $n_i\sqrt{3}\,a/2\pi$, where n_i is the number of carbon atoms along the circumference of the ith shell and a is the C–C bond length. For concentric tubes, $d_{(002)} = r_{i+1} - r_i = (n_{i+1} - n_i)\sqrt{3}\,a/2\pi$. Assuming that the change in the bond length is the same in every shell, one can arrive at the conclusion that $\Delta d_{002}/d_{002} = \Delta a/a$.
13. H. Zabel, in *Graphite Intercalation Compounds*, H. Zabel and S. A. Solin, Eds. (Springer-Verlag, Berlin, 1990), p. 101.
14. The *ab* plane linear compressibility of graphite was obtained by a linear fit to in-plane lattice parameter versus pressure data of R. W. Lynch and H. G. Drickamer [*J. Chem. Phys.* **44**, 181 (1966)] to 20 kbar.
15. M. S. Dresselhaus and G. Dresselhaus, *Adv. Phys.* **30**, 139 (1981).
16. N. J. Wu and A. Ignatiev, *Phys. Rev. B.* **28**, 7288 (1983).
17. S. C. Tsang, P. J. F. Harris, M. L. H. Green, *Nature* **362**, 520 (1993).
18. P. M. Ajayan *et al.*, *ibid.*, p. 522.
19. L. A. Girifalco and R. A. Lad, *J. Chem. Phys.* **25**, 693 (1956).
20. S. W. Bensen, *Thermochemical Kinetics* (Wiley, New York, 1976).
21. G. B. Adams, O. F. Sankey, J. B. Page, M. O'Keefe, D. A. Drabold, *Science* **256**, 1792 (1992).
22. R. C. Haddon, *ibid.* **261**, 1545 (1993).
23. S. H. Glarum, S. J. Duclos, R. C. Haddon, *J. Am. Chem. Soc.* **114**, 1996 (1992).
24. The origin of the enhanced diamagnetism will be discussed in a separate paper (A. P. Ramirez *et al.*, in preparation).
25. R. D. Heidenreich, W. M. Hess, L. L. Ban, *J. Appl. Crystallogr.* **1**, 1 (1968).
26. We thank M. J. Rosseinsky, R. Felder, J. E. Fischer, P. A. Heiney, R. Tycko, G. Dabbagh, D. J. Eaglesham, and A. J. Lovinger for useful discussions and technical assistance; J. E. Fischer for providing the HOPG sample; D. E. Cox for the use of his apparatus at Beam Line X7A, National Synchrotron Light Source (NSLS); and R. E. Smalley for samples and comments on the manuscripts. NSLS is supported by the U.S. Department of Energy, Division of Materials Sciences and Division of Chemical Sciences.

24 November 1993; accepted 1 February 1994

Changes in Atmospheric Circulation and Ocean Ice Cover over the North Atlantic During the Last 41,000 Years

P. A. Mayewski,* L. D. Meeker,† S. Whitlow, M. S. Twickler, M. C. Morrison, P. Bloomfield, G. C. Bond, R. B. Alley, A. J. Gow, P. M. Grootes, D. A. Meese, M. Ram, K. C. Taylor, W. Wumkes

High-resolution, continuous multivariate chemical records from a central Greenland ice core provide a sensitive measure of climate change and chemical composition of the atmosphere over the last 41,000 years. These chemical series reveal a record of change in the relative size and intensity of the circulation system that transported air masses to Greenland [defined here as the polar circulation index (PCI)] and in the extent of ocean ice cover. Massive iceberg discharge events previously defined from the marine record are correlated with notable expansions of ocean ice cover and increases in PCI. During stadials without discharge events, ocean ice cover appears to reach some common maximum level. The massive aerosol loadings and dramatic variations in ocean ice cover documented in ice cores should be included in climate modeling.

During the last glaciation, the North Atlantic region experienced major changes in climate relative to the Holocene (the most recent 10,000 years). The most obvious and dramatic of these changes consisted of variable length stadial (cold) and interstadial (milder) periods. The major ion series (*1*) collected as part of the Greenland Ice Sheet Project Two (GISP2) (72.6° N, 38.5° W, 3200-m elevation) provide a particularly sensitive monitor of these events. This multivariate suite of time series reveals a record of variability in the major soluble constituents of the atmosphere over Greenland (*2*, *3*) that can be used to interpret response to climate change (changes in atmospheric circulation and ocean ice cover extent) and the potential influence of several major climate forcing agents (dust loading, ocean ice cover, and ice sheet stability).

We analyzed the GISP2 calcium, chloride, sulfate, sodium, magnesium, potassium, ammonium, and nitrate ion series covering the last 41,000 years (Fig. 1). A previously identified antiphase relation between oxygen isotopes and dust (*4*, *5*) holds, to a variable degree, between oxygen isotopes and many ion species (Fig. 1). It is the common features among the multivariate ion species and the contrasting divergence from that commonality by individual ion records that provide the detailed view of atmospheric circulation over the North Atlantic that we discuss below.

Because the two primary sources for chemical species transported to the Greenland atmosphere are terrestrial dusts and marine surfaces (*2*), we focus here on changes in the chemical series that monitor these sources. Quantities for these two sources (Fig. 2) were estimated by partitioning (*6*) calcium, chloride, sulfate, sodium, magnesium, and potassium into sea salt and excess (total minus estimated sea salt) contributions. Excess quantities were then combined to provide an estimate of terrestrial dust. Stadials (low oxygen isotope events) are characterized by synchronous increases in both dust and sea salt, whereas relatively low concentrations of both components are typical of the interstadials (high oxygen isotope events).

Neither ammonium nor nitrate concentrations (Fig. 1) are accounted for in the dust and sea salt estimates. These two species represent less than 8% of the total soluble ionic loading of the atmosphere during the pre-Holocene and display only subtle to minimal variation in that portion of the record. Because interpretation of the concentration records is not straightforward (*7*), our discussion is limited to the remaining six GISP2 ion series.

Dust and sea salt concentrations differed significantly during the Holocene, stadials, and interstadials [including during the Bolling/Allerod (B/A)]: 11 and 17, 267 and 165, and 52 and 72 parts per billion (ppb), respectively. Ionic balance determinations revealed other differences. During the glacial period, at least 50% of the calcium was in the form of $CaCO_3$, with the remainder of the calcium and other cations in the form of compounds such as NaCl, NaNO3, $CaSO_4$, and $(NH_4)_2SO_4$ (*3*). This distribution is a significant departure from the

P. A. Mayewski, L. D. Meeker, S. Whitlow, M. S. Twickler, M. C. Morrison, Glacier Research Group, Institute for the Study of Earth, Oceans, and Space, University of New Hampshire, Durham, NH 03824, USA.
P. Bloomfield, Department of Statistics, North Carolina State University, Raleigh, NC 27695–8203, USA.
G. C. Bond, Lamont-Doherty Earth Observatory, Palisades, NY 10964, USA.
R. B. Alley, Earth System Science Center and Department of Geosciences, Pennsylvania State University, University Park, PA 16802, USA.
A. J. Gow and D. A. Meese, Cold Regions Research and Engineering Laboratory, Hanover, NH 03755, USA.
P. M. Grootes, Quaternary Isotope Laboratory, University of Washington, Seattle, WA 98195, USA.
M. Ram, Department of Physics, University of Buffalo, Amherst, NY 14260, USA.
K. C. Taylor, Desert Research Institute, University of Nevada System, Reno, NV 89506, USA.
W. Wumkes, Polar Ice Coring Office, University of Alaska, Fairbanks, AK 99775, USA.

*To whom correspondence should be addressed.
†Also at Department of Mathematics, University of New Hampshire, Durham, NH 03824, USA.

generally more acidic Holocene atmospheric conditions over Greenland. In addition to changes in the magnitude of mean dust and sea salt values, these series also display greatly enhanced decadal scale variations, most notable in the dust series during stadial events (Fig. 2). This evidence further substantiates previous findings of frequent, rapid (decadal scale), and massive atmospheric changes during the last ~41,000 years (3, 5, 8).

Although there was a general synchronous increase and decrease in sea salt and dust levels during stadials and interstadials, the two records differ in an important way. Sea salt levels appear much the same during all stadial events, but the dust record reveals important differences (Fig. 2). During several stadials [for example, around 40, 30, and 24 thousand years ago (ka)], excess calcium and excess sodium concentrations (as well as excess potassium and magnesium) (Fig. 1) were significantly higher than the general stadial background. These dust increases most likely reflect periods during which atmospheric circulation expanded to include new source regions over continents and continental shelves or intensified over such regions. Because sea salt levels do not increase concurrently, increased wind speed alone cannot account for the dust increase.

The chemical species were not transported to Greenland as single ion species but, rather, as components of chemical compounds carried within air masses having their own chemical signatures characteristic of source and transport histories. This suggests that multivariate time series analysis, with its capacity to describe and highlight differences and similarities among the species, may provide the most direct view of paleoatmospheres. For this reason, we investigated the joint behavior of the chemical species calcium, chloride, sulfate, potassium, magnesium, and sodium (Fig. 1) using analysis based on an empirical orthogonal function (EOF) (3, 9) decomposition [the ammonium and nitrate series were excluded from this analysis (7)].

In the EOF analysis, the data matrix (which measures $m = 6$ species by $N = 8450$ samples) is factored into the product of the $m \times m$ matrix V of eigenvectors of the correlation matrix and the $m \times N$ matrix W (9). The first EOF, EOF1, based on the product of the first column of V and the first row of W (9), displays the dominant multivariate chemical association among the series (Fig. 2). In this mode, all species have approximately the same (normalized) magnitude (eigenvector components are 0.41, 0.41, 0.40, 0.41, 0.42, and 0.42 for calcium, chloride, sulfate, potassium, magnesium, and sodium, respectively). This eigenmode explains 92% of the total variance in the combined six series. Components of the EOF that explain a large proportion of the variance in a multivariate series are commonly found to have important physical significance (3, 9). In this case, an underlying physical process capable of explaining such a high degree of variance and combining so many chemical species sources and transport histories must be a large-scale dominant feature of the atmospheric system. We propose, as for a similar glaciochemical association during the Younger Dryas (YD) (3), that EOF1 provides a description of the "background" atmosphere. Because EOF1 provides a linear model of an atmosphere in which all six species increase or decrease together in constant proportions, this background at-

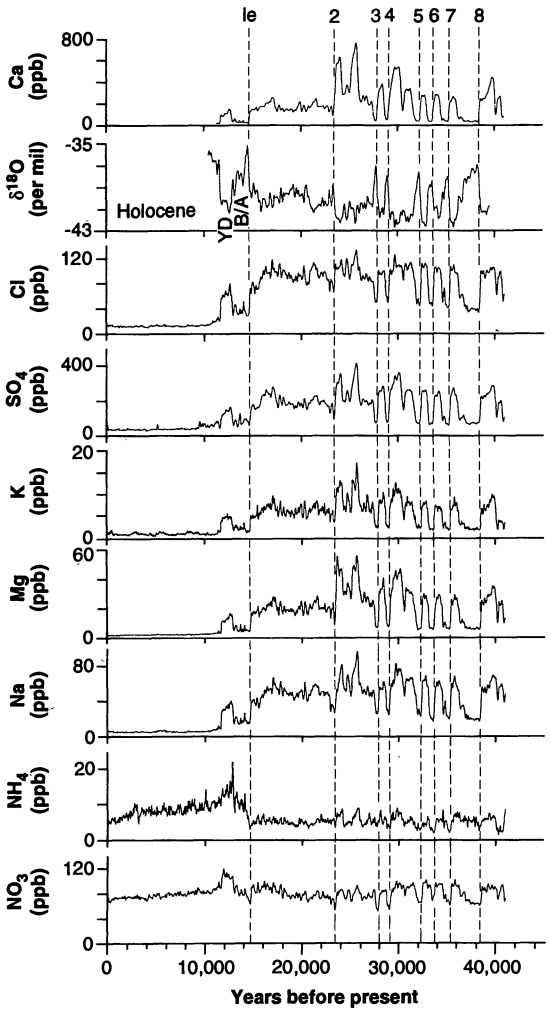

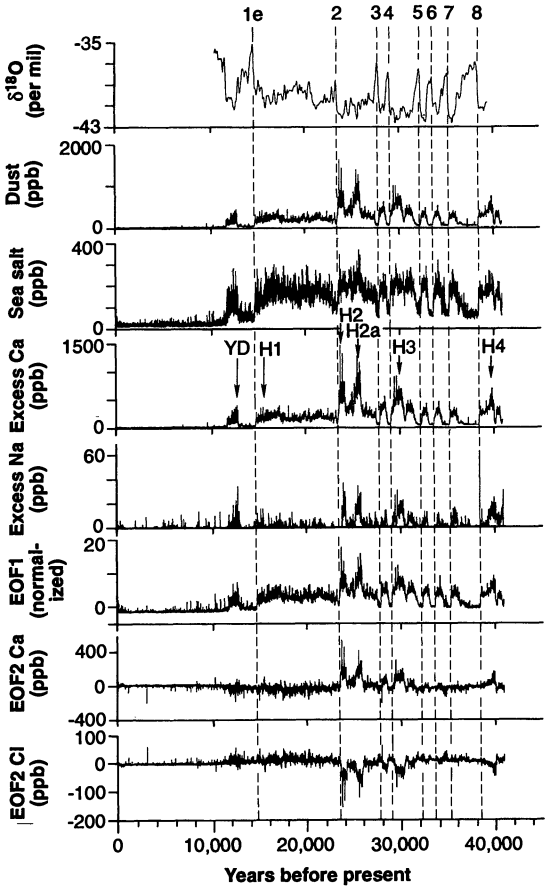

Fig. 1 (left). Robust spline smooth (*20*) versions (20% smoothing) of the original calcium, chloride, sulfate, sodium, magnesium, potassium, ammonium, and nitrate series for the period from the present to 41 ka (total number of samples, 8450). Sample resolution for the original series is ~2 years through the Holocene, a mean of 3.48 years within the Younger Dryas (YD) and the Bolling/Allerod (B/A), and ~3 to 15 years for the remainder of the record. Oxygen isotope values are presented as a robust spline smooth (20% smoothing) of the original 1 sample/m series. Dating is based on continuous multivariate annual layer counting (*8, 21*). Cumulative age errors are 2% (0 to 11.64 ka) and 5% (11.64 to 41 ka) (*8*). Interstadial number designation from (*22*). **Fig. 2 (right).** Oxygen isotopes (same as Fig. 1) followed by dust, sea salt, excess calcium, and excess sodium calculated from the original chemical series (*6*) plus EOF1 in normalized units (PCI) and EOF2 calcium and EOF2 chloride in their scaled form. Dating and interstadial designation are the same as Fig. 1. Heinrich events are listed as YD and H1 to H4 after (*16*) plus H2a postulated from this study.

mosphere is, by definition, a well-mixed atmosphere. For purposes of discussion, we define the normalized time series associated with EOF1 as the polar circulation index (PCI), a relative measure of the combined intensity and overall size of the circulation system that produces the well-mixed background atmosphere over Greenland.

The large-scale atmospheric circulation patterns capable of transporting sea salt and dust to central Greenland are dominated by westerly or meridional patterns in the circumpolar vortex. Important locations for the incorporation of sea salt and dust into these circulation patterns are the regions of strong cyclogenesis that form along marine and atmospheric thermal gradients (*10*). These are believed to have been significantly steepened by the radiative influence of ice sheets during the last glaciation (*11*). The presence of this continental ice cover also led to the increased production of sea ice in the North Atlantic (*12*). Thus, the sea salt measured in our record (Fig. 2) traveled from more distant marine surfaces during the glacial age portion of our record, and the increase in sea salt during this period of sea ice expansion must have been caused largely by intensified aerosol incorporation at the sea ice margin. Primary dust sources would, of course, have been south of the main ice cover and their incorporation or absence in air masses transported to Greenland would have signaled passage of this circulation to the south of the ice sheets or entirely over them (source region totally ice covered), respectively.

The relative influence of a well-mixed atmosphere (EOF1) compared to a more locally influenced atmosphere can be explored by examining the variance explained by the first EOF calculated over different time intervals. The EOF analyses over the Holocene, YD, B/A, all stadials combined, and all interstadials combined yield, essentially, the same dominant eigenvector (all normalized components approximately equal), whereas the variation among the six ion series explained by the first mode varies considerably. The percentages of total variance explained by the first EOF calculated for each of the different time periods are 51% (Holocene), 71% (YD), 66% (B/A), 72% (all interstadials combined), and 80% (all stadials combined).

From this analysis, it is clear that the relative influence of the dominant EOF is greater during cold periods (YD and stadials) than it is during the milder periods (Holocene, B/A, and interstadials). During the Holocene period, nearly 50% of the series variance is attributable to non-EOF1 processes involving air masses with other chemical signatures—for example, those containing primarily marine or primarily terrestrial species. A slightly increased role for EOF1 during the B/A and interstadial periods indicates an increase and growth in the well-mixed circulation pattern. During the colder periods, the well-mixed model becomes increasingly important, indicating a circulation pattern of such size and strength that intrusions to Greenland by less well mixed air masses are of minor importance.

When applied to the total 41-ka record, EOF1 explains 92% of the overall variance of the six chemical series. With such a dominant mode, the remaining eigenmodes would not, typically, be expected to be statistically distinguishable. However, in this instance, Bartlett's test (*13*) for equality of the five smallest eigenvalues is highly significant ($P < 0.0001$), and therefore, it is reasonable to examine the relations associated with other EOFs. Although the remaining variance, which is distributed among the other five EOFs, is of little significance in the multivariate frame, individual ion species do display significant deviations from the linear model.

Notably, EOF2 [based on the second column of V and second row of W (9)] explains 8% of the variance in both the calcium and the chloride series (EOF1 and EOF2 account for approximately 98% of the total variance of the calcium and chloride series). Unlike EOF1, the predominantly terrestrial calcium and the predominantly marine chloride species are oppositely loaded on EOF2. This implies that positive excursions from the mean for this component of calcium are accompanied by negative excursions from the mean by chloride values (Fig. 2). Note that this estimate of chloride behavior was calculated independently from our chemical determination for sea salt (6). The EOF2 series reveals several prominent periods when calcium was high, chloride was low, and sea salt remained relatively unchanged (Fig. 2). These periods coincide with those already identified as having had increased dust levels (around 40, 30 and 24 ka, for example) as a result of changes in circulation or intensified transport. Periods during which there was a coincident decrease in EOF2 chloride reflect times when sea salt was transported from even more distant sources than predicted by the PCI model (greater fractionation of the sea salt aerosol and progressively less chloride). Therefore, periods characterized by relatively high sea salt concentrations that are accompanied by decreased EOF2 chloride levels monitor expansions of ocean ice cover relative to the PCI model.

To investigate the type of ocean ice cover influence observed in our record (sea ice or iceberg), we included the location of Heinrich (H) layers [marine layers rich in ice-rafted debris and poor in foraminifera (*14*) that represent massive iceberg discharge events and attendant cooling of surface waters (*15*)]. Marine H layer timing has already been matched to Greenland Ice Core Project (GRIP) oxygen isotope events to reveal cooling cycles that culminate in these iceberg discharge events (*16*). For the period examined here, GRIP and GISP2 oxygen isotope events coincide exactly (*17*), allowing the placement of the H layer events on Fig. 2.

All stadial events are characterized by increases in sea salt and dust, but prominent increases in excess calcium and excess sodium (Fig. 2) are coincident with three H events (H4, H3, and H2). During these events, EOF2-derived calcium and chloride components show large increases and de-

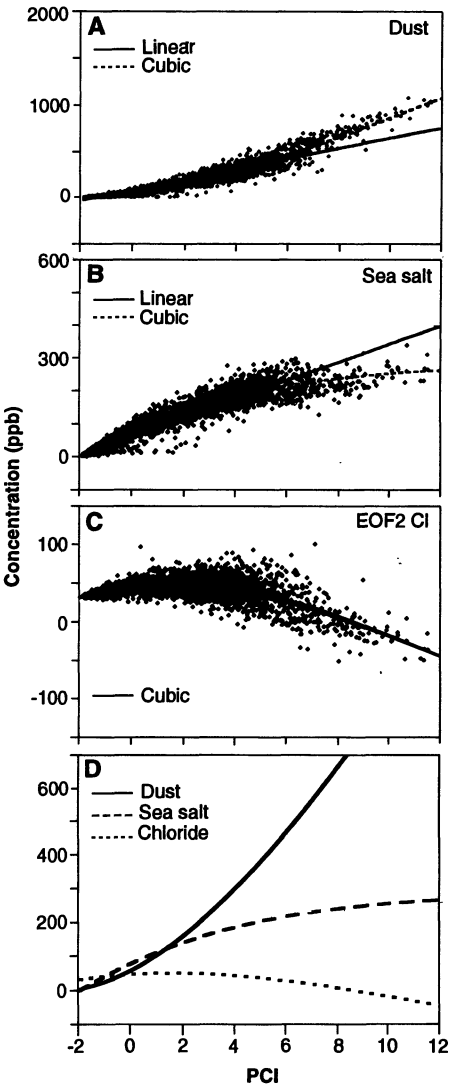

Fig. 3. Concentration of (**A**) dust, (**B**) sea salt, and (**C**) EOF2-derived chloride versus PCI (normalized EOF1). N = 8540 points per series. Linear and cubic approximations to the data are included. Because EOF2 chloride is uncorrelated to EOF1, a linear approximation is not presented for (C). (**D**) Summary comparison of the cubic approximations.

creases, respectively. The two remaining H events believed to occur during the study period (H1 and YD) (*16*) are characterized only by increased excess sodium, which may not be surprising because H1 was previously suggested to have a different ice sheet–climate relation than other H events (*16*) and YD, unlike other H events, occurred during the deglaciation. One H-like event (H2a), characterized by the same chemical signatures as H4 through H2, is also evident in our record. Further examination of the marine record may reveal this H-like event. All of the H and H-like events except H1 and YD were accompanied by higher PCI values and, on the basis of calcium and chloride EOF2 records, relatively expanded ocean ice cover.

As discussed above, the PCI describes the behavior of a linear model of the six species concentrations. The climate system, however, may be largely nonlinear, and linear approximations based on one or two EOFs may obscure important nonlinearities in the records. To explore this possibility, we compared the independently derived dust and sea salt and the EOF2 chloride series with the PCI series (Fig. 3). Nonlinear departures from the PCI model are confirmed by cubic polynomial regression models ($R^2 = 0.96$ for each series and coefficient $t > 10$ in each instance).

These regression curves provide the basis for an objective classification of Greenland atmospheric conditions (Fig. 4). For low values of the PCI, the sea salt mean value is somewhat larger than that of the dust. This difference increases to a maximum at PCI $\approx$ 0, which we take as the upper limit defining one atmospheric state. The difference between the two curves then decreases until they intersect at PCI $\approx$ 1.5, which we define as the upper limit for another atmospheric state. For larger values of PCI, the regression curve for the dust series lies above that of the sea salt series. At PCI values of ~5, the cubic regression curves intersect their respective linear approximations and begin a rapid departure from linear growth (dust increases while sea salt and EOF2 chloride decrease). Accordingly, PCI = 5 is taken as the boundary dividing two other atmospheric states.

All stadials attain a PCI $\geq$ 5, but only stadials associated with H and H-like events have PCI values that rise markedly above 5 over periods spanning more than decades (single spikes represent sample resolutions of ~3 to 15 years). At PCI $\geq$ 5, there is significantly more dust than sea salt in the atmosphere over Greenland, and sea salt and EOF2 chloride concentrations are lower than predicted by the model (longer transport results from expanded ocean ice cover and more fractionation of the sea salt aerosol). The ocean ice cover expansions

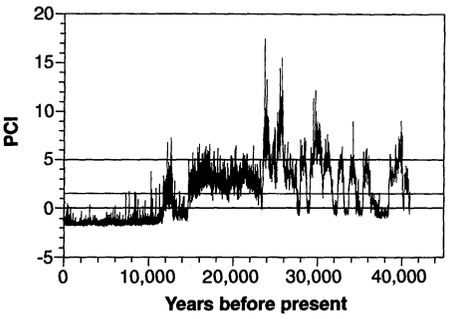

Fig. 4. Atmospheric states plotted on the PCI model (EOF1 in normalized units).

documented by these changes and attendant changes in albedo would have contributed significantly to an intensification and expansion of the circulation system feeding Greenland. Our record, therefore, reveals the atmospheric response to these massive iceberg discharge events (ice sheet instabilities). Because dust concentrations exceed those predicted in the PCI linear model, it is possible that new continental and continental-shelf source regions were incorporated into this circulation. By the termination of H2, the most dramatic iceberg discharge events appear to have ceased (Fig. 4).

Values of PCI from ~1.5 to 5 include most of the timing of the non-H related stadials and much of the YD. Sea salt and EOF2 chloride are higher than expected in the linear model and dust is lower, although there is still more dust than sea salt in the atmosphere. Sea ice extent was less relative to periods when PCI values >5 existed as demonstrated by relatively high sea salt associated with relatively high EOF2 chloride values (less fractionation). However, dust levels are lower than expected, suggesting relatively reduced areal extent of the circulation system feeding Greenland (consistent with decreased sea ice cover). All of the stadials not associated with H layers appear to reach a common upper level of PCI and sea salt at some time during their existence, suggesting a maximum possible expansion of sea ice extent, exclusive of further cooling induced by iceberg discharge, presumably controlled by the basin configuration of the North Atlantic.

Values of PCI between ~0 and 1.5, in general, characterize the periods of stadial onset and decline [relatively rapid periods on the order of decades (*3*, *5*, *8*)]. Although sea salt and dust concentrations gradually converge until PCI $\approx$ 1.5, when dust levels rise above sea salt, the dust and sea salt changes generally follow the linear PCI model. The EOF2 chloride is high relative to the PCI model, suggesting reduced sea ice extent relative to the model. The generally linear buildup of both dust and sea salt suggests that atmospheric mixing is the more dominant process controlling atmospheric composition at these times. Hence, the periods of rapid onset and decay of stadials appear to be characterized by turbulent atmospheric conditions. Because dust levels exceed those for sea salt at PCI $\approx$ 1.5 and yet both continue to increase above this value, there must be a control on sea salt incorporation. We suggest that the control is sea ice growth, which builds during periods of stadial onset and decays during periods of stadial decline. At ~1.5, sea ice extent is large enough that the transport distance from the sea ice edge to Greenland limits the receipt of sea salt to Greenland.

The Holocene, almost all of the B/A, and all interstadials are characterized by PCI < 0. These periods display the greatest overall difference from the PCI model because the linear model calculation is dominated by the pre-Holocene record.

The presence of continental ice sheets during the last glaciation and YD provided conditions suitable for relatively unstable conditions (massive and rapid changes in the size and intensity of the PCI and ocean ice cover) relative to the Holocene. Increases in the PCI were accompanied by increased levels of terrestrial and sea salt aerosols. These massive and rapid aerosol loading events may have contributed to shielding of incoming solar radiation and may partly explain the duration of the stadial events. The rapid, massive fluctuations in sea ice and iceberg extent that we document may have played a major role in the radiation balance and thermohaline circulation of the ocean. Changes in ocean ice cover have the potential to significantly magnify surface and lower tropospheric temperature over marine surfaces and consequently affect meridional temperature gradients and zonal atmospheric circulation (*18*). For all stadials, except those related to iceberg discharge events, there appears to have been an upper limit to sea ice extent. It remains to be seen whether the iceberg discharges were driven by external climate forcing or internal ice sheet dynamics and whether the sea ice fluctuations were purely a response to climate change or a major contributor. However, the changes in atmospheric circulation and ocean ice cover monitored by our glaciochemical records appear to respond rapidly enough to yield direct evidence of the effects of climate forcing, and future study of such events should prove valuable in constraining the significance and character of climate forcing agents.

REFERENCES AND NOTES

1. All chemical sampling and analysis undertaken on the GISP2 core was done with specially adapted glaciochemical techniques [P. A. Mayewski *et al.*, *Nature* **346**, 554 (1990); C. F. Buck, *J. Chromatogr.* **594**, 225 (1992)].

2. P. A. Mayewski *et al.*, *Ann. Glaciol.* **14**, 186 (1990); P. A. Mayewski *et al.*, *J. Geophys. Res.* **98**, 12839 (1993).
3. P. A. Mayewski *et al.*, *Science* **261**, 195 (1993).
4. C. U. Hammer *et al.*, in *Greenland Ice Core: Geophysics, Geochemistry, and the Environment*, C. C. Langway, H. Oeschger, W. Dansgaard, Eds. (Geophys. Monogr. **33**, American Geophysical Union, Washington, DC, 1985), pp. 90–94.
5. K. C. Taylor *et al.*, *Nature* **361**, 432 (1992).
6. The sea salt components of each potential sea salt source species (calcium, chloride, sulfate, sodium, magnesium, and potassium) (*2*) were estimated by an iterative process during which each sample was tested to determine which source species was the most conservative (limiting). In 23% of the cases, chloride was limiting, and for 76%, sodium was limiting. We calculated sea salt corrections per sample using the limiting species. Volcanic sources for sulfate were not removed from the calculation because most of the stadials were sampled at a resolution of ~3 to 15 years and volcanic events are obscured at this resolution. Subtraction of the sea salt component from the total for each species provided an excess value. The excess quantity was derived from crustal sources (*2*).
7. The ammonium and nitrate series can only be interpreted after annual snow accumulation rate measurements have been calculated for the GISP2 ice core because, unlike the other species measured in this study, ammonium and nitrate flux (accumulation times concentration) series differ notably from their concentration series (*3*) as a consequence of the depositional and postdepositional processes that are unique to these species (*19*).
8. R. B. Alley *et al.*, *Nature* **362**, 527 (1993).
9. J. P. Peixoto and A. H. Oort, *Physics of Climate* (American Institute of Physics, Woodbury, NY, 1992). The EOF analysis represents the $m \times N$ data matrix ($m = 6$, $N = 8450$) by $X = M + DVW$, where M is the (row-constant) matrix of estimated mean values, D is a diagonal matrix containing the estimated standard deviations of the series, V is the $m \times m$ matrix of eigenvectors of the correlation matrix of X, and W is the $m \times N$ matrix (with uncorrelated rows) describing the temporal contributions of the eigenvectors to the observations (in the columns) of X. The first EOF is EOF1 $= M + DV_1W_1$, where V_1W_1 is the rank 1 matrix product of the first column of V with the first row of W. It, therefore, represents synchronous behavior among the m series with each series following a rescaled version of the $1 \times N$ series W_1 (described as PC1) (Fig. 2).
10. H. H. Lamb, *Q. J. R. Meteorol. Soc.* **81**, 172 (1955).
11. A. J. Broccoli and S. Manabe, *Geogr. Phys. Quaternaire* **41**, 291 (1987).
12. W. F. Ruddiman and A. McIntyre, *Quat. Res.* **16**, 125 (1981).
13. I. H. Bernstein, *Applied Multivariate Analysis* (Springer-Verlag, New York, 1988).
14. H. Heinrich, *Quat. Res.* **29**, 142 (1988).
15. G. Bond *et al.*, *Nature* **360**, 245 (1992).
16. G. Bond *et al.*, *ibid.* **365**, 143 (1993).
17. P. A. Grootes *et al.*, *ibid.* **366**, 552 (1993).
18. R. E. Moritz, J. A. Curry, A. S. Thorndike, N. Untersteiner, Eds., *SHEBA (Surface Heat Budget of the Arctic Ocean)* (University of Washington, Seattle, WA, 1993).
19. P. A. Mayewski and M. R. Legrand, *Nature* **346**, 258 (1990).
20. P. Bloomfield and W. L. Steiger, *Least Absolute Deviations: Theory, Applications, and Algorithms* (Birkh, Boston, MA, 1983), pp. 131–151. The robust spline minimizes a weighted combination of the integral of the squared second derivative and the sum of absolute deviations about the curve.
21. D. Meese *et al.*, U.S. Army Cold Regions Research and Engineering Laboratory Report, in press.
22. W. Dansgaard *et al.*, *Nature* **364**, 218 (1993).

23. We thank J. Dadah, F. Casella, K. Moran, S. O'Brien, J. Putscher, C. Schuman, J. Thomas, K. Welch, Q. Yang, the Polar Ice Coring Office, the GISP2 Science Management Office, and the 109th Air National Guard. This research is supported by the U.S. National Science Foundation Office of Polar Programs and Division of Mathematical Sciences.

15 June 1993; accepted 2 February 1994

Gallium Arsenide Transistors: Realization Through a Molecularly Designed Insulator

Phillip P. Jenkins, Andrew N. MacInnes, Massood Tabib-Azar,* Andrew R. Barron†

A GaAs-based transistor, analogous to commercial silicon devices, has been fabricated with vapor-deposited cubic GaS as the insulator material. The *n*-channel, depletion mode, GaAs field-effect transistor shows, in addition to classical transistor characteristics, a channel mobility of 4665.6 square centimeters per volt per second, an interfacial trap density of 10^{11} per electron volt per square centimeter, and a transconductance of 7 millisiemens for a 5-micrometer gate length at a gate voltage of 8 volts. Furthermore, the GaAs transistor shows an on-to-off resistance ratio comparable to that of commercial devices.

Gallium arsenide (GaAs) has over the last decade become the semiconductor material of choice in a number of "niche" applications: for example, optoelectronics [lasers and light-emitting diodes (LEDs) for optical communications and consumer electronics], microwave monolithic integrated circuits (MIMICs) (used in wireless communications such as cellular telephones), and very high frequency analog and digital signal-processing circuits (used for high–data-rate real-time processing) (*1–3*). However, except for specialty, primarily military, applications, GaAs has been unable to compete with silicon technology in the area of digital electronics.

At present, logic circuits, such as those used in the central processing unit of a modern personal computer, are based on silicon complimentary metal-oxide-semiconductor (CMOS) circuits, the basic component of which is a metal-oxide-semiconductor field-effect transistor (MOSFET) (*4*). Requirements for the development of the next level in digital electronics include greater speed, lower power consumption, and the incorporation of optoelectronics directly into the circuits (*5*). It has long been known that GaAs and related III-V compound semiconductors are faster than silicon (up to six times), and because of their direct band gap, they have the potential for the development of on-chip optoelectronics. However, present GaAs technology in the field of digital electronics (logic circuits) is limited by the inability to manufacture a GaAs analog of a MOSFET device, that is, a metal-insulator-semiconductor FET (MISFET) (*6*).

Present GaAs FET devices are metal-semiconductor FETs (MESFETs), which while faster than silicon MOSFETs suffer from several drawbacks. First, MESFETs consume more power than MISFETs. The undesirable power consumption is one of the barriers to very large scale integration (VLSI) of GaAs-based circuits. Second, the lack of any insulator between the gate and the channel results in large current conduction through the gate electrode. To circumvent the problems of current leakage across the gate, device architects must implement highly intricate and complex circuit designs. Because both of these problems are inherent in MESFET devices and are not readily solved, the entry of GaAs into the mainstream of high-performance digital electronics has been inhibited. To overcome the limitations of both silicon MOSFETs and GaAs MESFETs, it is thus necessary to develop GaAs-based MISFET devices.

The MISFET was first proposed in the 1930s by Lilienfeld (*7*) and Heil (*8*). We acknowledge earlier attempts to produce a GaAs MISFET (*9*), but a combination of either poor gate passivation (*10*) and insulating properties (*11*) or processing difficulties have precluded its realization (*12*). An ideal gate material for a MISFET device would have the following properties: a high band gap (insulating) material with low electrical conduction, a large breakdown field, good chemical and operational stability, and good interface properties with the chosen semiconductor (*13*). Furthermore, the following properties, although not nec-

P. P. Jenkins, NYMA, 2001 Aerospace Parkway, Brookpark, OH 44142, USA.
A. N. MacInnes, Gallia, Inc., Weston, MA 02193, USA.
M. Tabib-Azar and A. R. Barron, Department of Chemistry, Harvard University, Cambridge, MA 02138, USA.
*On sabbatical leave from the Department of Electrical Engineering and Applied Physics, Case Western Reserve University, Cleveland, OH 44106, USA.
†To whom correspondence should be addressed.